# Five-Parameter Fluorescence Imaging: Wound Healing of Living Swiss 3T3 Cells

Robbin DeBiasio, Gary R. Bright, Lauren A. Ernst, Alan S. Waggoner, and D. Lansing Taylor

Department of Biological Sciences, Center for Fluorescence Research in Biomedical Sciences, Carnegie Mellon University, Pittsburgh, Pennsylvania 15213

*Abstract.* Cellular functions involve the temporal and spatial interplay of ions, metabolites, macromolecules, and organelles. To define the mechanisms responsible for completing cellular functions, we used methods that can yield both temporal and spatial information on multiple physiological parameters and chemical components in the same cell. We demonstrated that the combined use of selected fluorescent probes, fluorescence microscopy, and imaging methods can yield information on at least five separate cellular parameters and components in the same living cell. Furthermore, the temporal and spatial dynamics of each of the parameters and/or components can be correlated with one or more of the others. Five parameters were investigated by spectrally isolating defined regions of the ultraviolet, visible, and near-infrared spectrum based on five distinct fluorescent probes. The parameters included nuclei (Hoechst 33342), mitochondria ($diIC_1$-[5]), endosomes (lissamine rhodamine B-dextran), actin (fluorescein), and the cell volume (Cy7-dextran). Nonmotile, confluent Swiss 3T3 cells did not show any detectable polarity of cell shape, or distribution of nuclei, endosomes, or mitochondria. These cells also organized a large percentage of the actin into stress fibers. In contrast, cells migrating into an in vitro wound exhibited at least two stages of reorganization of organelles and cytoplasm. During the first 3 h after wounding, the cells along the edge of the wound assumed a polarized shape, carried the nuclei in the rear of the cells, excluded endosomes and mitochondria from the lamellipodia, and lost most of the highly organized stress fibers. The cell showed a dramatic change between 3 and 7 h after producing the wound. The cells became highly elongated and motile; both the endosomes and the mitochondria penetrated into the lamellipodia, while the nuclei remained in the rear and the actin remained in less organized structures. Defining the temporal and spatial dynamics and interplay of ions, contractile proteins, lipids, regulatory proteins, metabolites, and organelles should lead to an understanding of the molecular basis of cell migration, as well as other cellular functions.

THE successful completion of cell functions such as endocytosis, cell division, and cell motility involves the temporal and spatial interplay of ions, metabolites, macromolecules, and organelles (Taylor et al., 1986). A major goal of cell biology is to quantify these cellular parameters and components and to correlate the distinct chemical and structural changes that are responsible for specific cell functions. However, the complex chemical dynamics of living cells have been difficult to study at the molecular level due to the lack of specific and sensitive methods to measure these physiological parameters in living cells. Research in cell biology has therefore been focused on the biochemical analyses of isolated cellular components and on light and electron microscopic characterization of fixed cells. Unfortunately, these and related methods, although valuable, cannot be used to investigate the dynamic chemical processes that take place over time in different regions of living cells. Methods are needed to measure multiple physiological parameters in the same individual cells yielding both temporal and spatial information.

Fluorescence microscopy, in conjunction with the multitude of sensitive fluorescent probes now available, offers a powerful approach for gathering complex chemical and molecular information from single living cells (Taylor and Wang, 1980). The growing list of fluorescent probes include protein (see Wang et al., 1982; Taylor et al., 1984, 1986) and lipid analogs (Pagano and Longmuir, 1983), antibodies (Kreis and Birchmeier, 1983), nucleic acids (Latt et al., 1984), and physiological indicators (Waggoner, 1986; Tsien et al., 1982). Advances in instrumentation have allowed this methodology to evolve into a sensitive and specific tool (Chance, 1963; West, 1969; Kohen et al., 1981; Axelrod et al., 1976; Jacobson et al., 1976; Agard and Sedat, 1983; Tanasugarn et al., 1984; Arndt-Jovin et al., 1985; Benson et al., 1985; Lanni, 1986; Salmon and Wadsworth, 1986; Taylor et al., 1986; Bright et al., 1987).

Fluorescence imaging microscopy has evolved out of the applications of low light level video-imaging methods (Rose and Loewenstein, 1975; Willingham and Pastan, 1978; Reynolds and Taylor, 1980; Taylor and Wang, 1978) and has been

Table I. Filter Sets*

| Fluorescent probe | Wavelengths (nm) | | | | | |
| | Excitation | | Dichroic | Emission | | |
| | Center | Bandpass‡ | 50%§ | Center | Bandpass | Source |
|---|---|---|---|---|---|---|
| Hoechst 33342 | G350‖ | 56 | 395 | 420 | LP** | Z‡‡ (487701) |
| Fluorescein actin | 485 | 20 | 510 | 542 | 45 | Z (487717) |
| Lissamine rhodamine-β–dextran | 546‖¶ | 12 | 580 | 590 | 40 | Z-Excitation Z-Dichroic Ω-Emission |
| dilC₁(5) | 615 | 30 | 650 | 675 | 50 | Ω§§ |
| Cy7-dextran | 720 | 40 | 758 | 785 | 50 | Ω§§ |

* All filters are interference filters unless otherwise indicated.
‡ Total bandpass at half-maximum transmittance.
§ Wavelength of half-maximal transmittance.
‖ This is a colored glass filter.
¶ This filter set consists of a combination of two interference filters, a long pass and a short pass.
** This is a glass long-pass filter.
‡‡ Zeiss.
§§ Omega Optical, Inc., Brattleboro, VT.

influenced by video-enhanced contrast microscopy (Allen and Allen, 1983; Inoue, 1981; Allen et al., 1981). Fluorescence imaging microscopy allows the acquisition of multiple images with different pairs of excitation and emission wavelengths over a relatively short period of time (Tanasugarn et al., 1984; Taylor et al., 1986). The separate spectral images can be manipulated by a variety of image processing methods and analyzed individually or in combination. This approach permits the quantitation of temporal and spatial changes of each separate parameter, as well as correlations of multiple parameters. For example, the spatial and temporal dynamics of cellular parameters such as pH, pCa, membrane potential, distribution of selected fluorescent analogs, and whole organelles can be analyzed in the same living cell by acquiring a series of images for each fluorescent probe. Therefore, a multiple parameter "map" of living cells can be constructed.

The present paper demonstrates the ability to analyze five different cellular parameters in the same living cell based on the spectral isolation of four commercially available fluorophores and one new fluorescent probe ranging from the UV to the near-infrared region of the spectrum. The polarized

movements of Swiss 3T3 cells migrating into a wound area is used to correlate the temporal and spatial changes of selected parameters. Furthermore, the wide range of applications of this general approach is discussed.

## Materials and Methods

### Cell Culture and Preparation

Swiss 3T3 fibroblast cells (ATCC-CCL92) from the American Type Culture Collection (Rockville, MD) were cultured in DME (Gibco, Grand Island, NY), buffered with 2 mg/ml sodium bicarbonate, pH 7.4, (base; b-DME), and supplemented with 50 U/ml penicillin, 0.05 mg/ml streptomycin, and 10% calf serum (complete; c-DME).

To maintain stock cultures at a subconfluent density, 3T3 cells were subcultured every 3 d by trypsinization in 0.05% trypsin and 0.02% EDTA in Ca-Mg-free saline (Gibco). All cell cultures were incubated in a humidified 5% $CO_2$ environment at 37°C. Cell passage number ranged from 120 to 124.

For the five-parameter study, $\sim$3 × 10⁴ 3T3 cells were seeded into 100-mm tissue culture dishes (Corning Glass Works, Corning, NY) in c-DME. Subconfluent dishes were used 3–4 d after plating.

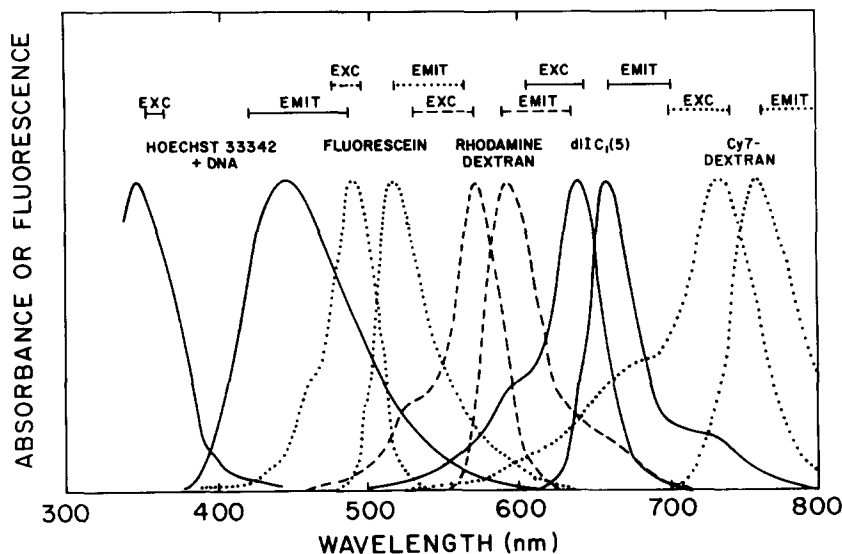In preparation for the wound-healing study, $\sim$1.0 × 10⁵ 3T3 cells were



Figure 1. Excitation and emission profiles of the five fluorophores used to label the cells for multiple parameter analysis.

*Table II. Selected Probes for Multiple-Parameter Imaging*

| Cellular parameter | Fluorescent probe | $\lambda_{ex}^{max}$ | $\lambda_{em}^{max}$ |
|---|---|---|---|
| Covalent labeling | Fluorescein-(ITC, DCT, OSu, MAL, IA) | 490 | 520 |
| Reagents*,‡‡ | Eosin-ITC | 522 | 560 |
| | Erythrosin-ITC | 540 | 560 |
| | TRITC | 554 | 573 |
| | XRITC | 582 | 601 |
| | MRITC | 540 | 577 |
| | X-RED-OSu | 580 | 600 |
| | Lissamine rhodamine-B-SCl | 570 | 590 |
| | Texas Red | 596 | 620 |
| | Cy3-OSu (or -IA, ITC) | 550 | 570 |
| | Cy5-ITC (or -IA, OSu) | 650 | 670 |
| | Cy7-OSu (or -IA, ITC) | 750 | 770 |
| | Phycoerythrin R | 480–565 | 578 |
| | Phycoerythrin B | 545–565 | 575 |
| | Allophycocyanine | 650 | 660 |
| | NBD-Cl | 460–490 | 520–550 |
| | Dansyl-Cl | 340 | 530–550 |
| pH | BCECF High pH/Low pH | 450:490 | 520 |
| Ca | Fura 2 with Ca⁺⁺/without Ca⁺⁺ | 335:360 | 510:515 |
| | Indo 1 with Ca⁺⁺/without Ca⁺⁺ | 330:350 | 405:485 |
| Membrane potential | | | |
| "Fast"‡ | WW781 | 620–633 | 640–660 |
| | RH414 | 520 | 600–700 |
| "Slow"‡ | diOCₙ(3) | 483 | 499 |
| | dilC₃(3) | 546 | 563 |
| | dilC₂(5) | 646 | 668 |
| | dilC₁(7) | 741 | 768 |
| | Rhodamine 123 | 485 | 530 |
| DNA§ | Hoechst 33342 | 340 | 450 |
| | DAPI | 350 | 470 |
| | Ethidium Br | 350, 525 | 620 |
| | Propidium iodide | 350, 535 | 625 |
| | Acridine orange | 480 | 520 |
| | Pyronine Y | 563 | 573 |
| RNA‖ | Acridine orange | 440–470 | 650 |
| | Pyronine Y | 470 | —¶ |
| Lipid** | Anthroyl stearates | 361, 381 | 446 |
| | NBD ceramide | 465 | 515 |
| | Dansyl phosphatidylethanol | 335 | 515 |
| | Nile red | 510 | 530 |
| | diOC₁₄₋₂₂(3) | 485 | 500 |
| | dilC₁₄₋₂₂(3) | 546 | 565 |
| | dilC₁₄₋₂₂(5) | 647 | 670 |

* In most cases the wavelengths given are for a labeled material rather than for the reactive dye. Many of the fluorophores listed have spectra that are sensitive to the microenvironment of the probe, thus the wavelengths listed are only approximate.
‡ Wavelengths given for dye in ethanol, which is a useful solvent to model the environment of membrane-bound probe.
§ Wavelengths given for dye bound to DNA.
‖ Single-stranded RNA.
¶ Very low quantum yield relative to probe bound to DNA.
** Wavelengths for probe bound to phosphatidylcholine vesicles or another lipid environment.
‡‡ The following abbreviations are used: *ITC*, isothiocyanate; *OSu*, succinimidyl; *DCT*, dichlorotriazinylamino; *MAL*, maleimido; *IA*, iodoacetamido; *SCl*, sulfonylchloride; *TRITC*, tetramethylrhodamine isothiocyanate; *XRITC*, rhodamine × isothiocyanate; *MRITC*, morpholinorhodamine isothiocyanate; *NBD*, nitrobenzoxadiazole; *BCECF*, biscarboxyethylcarboxyfluorescein.

seeded into 60-mm tissue culture dishes (Corning Glass Works) containing 40-mm round glass coverslips (Bellco Glass, Inc., Vineland, NY). Confluent monolayers on coverslips were obtained in 2 d. Coverslips were used on the third day after monolayers were confluent for 24 h.

## Fluorescent Probes

Multiparameter analysis was made possible by using five spectrally distinct fluorescent probes ranging from the UV to the near-infrared region of the spectrum. Table I and Fig. 1 provide complete filter set information and excitation/emission profiles for each fluorescent probe.

Hoechst 33342 (Sigma Chemical Co., St. Louis, MO), a DNA-specific probe, was used as a nuclear stain. Actin was purified from rabbit back muscles, gel filtered, and labeled with 5-iodoacetamidofluorescein (AF-actin)[1]

1. *Abbreviation used in this paper*: AF-actin, 5-iodoacetamidofluorescein.

(Molecular Probes, Inc., Eugene, OR) as previously described (Wang and Taylor, 1980). Lissamine rhodamine-B-dextran, (dextran mol wt 10,000; Molecular Probes, Inc.), labeled the intracellular vesicles. The cationic potential sensitive cyanine dye, diIC₁(5), was used as a probe for mitochondria (Waggoner, 1979; Cohen et al., 1981). The cyanine probe, Cy7-isothiocyanate (see Table II) (Mujumdar, R. B., L. A. Ernst, S. R. Mujumdar, and A. S. Waggoner, manuscript submitted for publication), was coupled to aminoethylcarboxymidomethyl-dextran (dextran mol wt 10,000; Pharmacia Fine Chemicals, Piscataway, NJ). Cy7-dextran loaded into the cytoplasm served as a volume indicator and delineated the thin peripheral edges of the cells.

## Wounding Technique

The wound-healing model (Todaro et al., 1967) was used to obtain polarized 3T3 cells. While examining the confluent coverslip on an inverted light microscope, the 3T3 cell monolayer was wounded by creating a vertical, ~1 mm-wide slash through the cell sheet using a tapered, non-abrasive tool. The wound edges were trimmed and retracted cell aggregates were removed, leaving a clean front edge. Straight, uniform wound edges enhanced parallel forward cell migration by decreasing areas available for multidirectional movement. The culture was returned to the 37°C incubator for a 10–15-min recovery period. The coverslip was gently washed with c-DME, 37°C, to remove cellular debris.

## Labeling Procedure

*Five-Parameter Study.* The scrape-loading technique (McNeil et al., 1984) was used to label the cytoplasm of a large number of 3T3 cells with the volume indicator Cy7-dextran. Briefly, this method involved harvesting adherent subconfluent 3T3 cells plated on 100-mm tissue culture dishes by scraping with a rubber policeman in the presence of a 13 mg/ml concentration of Cy7-dextran in a 150-mM KCl, 5 mM Hepes solution. Scraped cells were collected and washed twice in b-DME, 4°C, and plated at a low density in c-DME in 60-mm dishes containing 40-mm round glass coverslips. Cultures were incubated for 18 h to obtain well-spread single cells labeled with Cy7-dextran. This labeling procedure yielded a 50% cellular recovery rate with 50–70% of the recovered cells labeled with suitable fluorescence levels of Cy7-dextran.

Endosomes were labeled by fluid-phase pinocytosis using a fluorescent dextran solution. The coverslips were incubated in c-DME containing a 3.5 mg/ml concentration of lissamine rhodamine-B-dextran for 2 h at 37°C, 5% $CO_2$. The dishes were washed multiple times with c-DMEM and returned to the incubator for a 15-min recovery period.

The cells were microinjected with AF-actin (Amato et al., 1983) in the presence of b-DME. Best results of incorporation of AF-actin were obtained by using low passage 3T3 cells, and AF-actin (dye/protein ratio of 0.8) at a concentration of 4 mg/ml in an injection buffer of 0.05 mM $MgCl_2$, 0.1 mM ATP, 0.1 mM dithiothreitol (DTT), and 2 mM Pipes. Injected cells were given a minimum recovery period of 2 h at 37°C in c-DME.

Coverslips were incubated at 37°C for a minimum of 20 min in c-DMEM containing 7.5 × 10⁻⁷ M diIC₁(5) and 7.5 µg/ml Hoechst probe to label the mitochondria and the nuclei. The solution containing the membrane potential dye was not removed from the coverslip until immediately before mounting to delay the loss of the mitochondrial signal (2.5–3.5 h post removal) due to the diffusion gradient of the membrane potential dye from the cell into the chamber medium (Cohen et al., 1981).

The washed coverslips were mounted in modified Sykes–Moore chambers (Bellco Laboratories) (Bright et al., 1987) using phenol red-free c-DME (Gibco) which had been equilibrated for a minimum of 18 h in a 37°C, 5% $CO_2$ incubator.

*Wound-healing Study.* The scrape loading technique involving Cy7-dextran was not used in this study because the cellular processes examined after wounding are dependent on quiescent, density arrested cells, and cells used after scrape loading were plated for <24 h. After confluent monolayers of unlabeled 3T3 cells on coverslips were wounded, the vesicles, actin, mitochondria, and nuclei were labeled with the same fluorescent probes in the same sequence detailed above, with the exceptions of incubation in lissamine rhodamine-B-dextran solution for 1.75 h, and the recovery period after

AF-actin injection was 1 h. These modifications were made to observe early cell migration into the wound area. Polarized cells at selected wound sites were examined 4–7 h after wounding.

*Digital-Image Microscopy.* The microscope imaging system used to generate, acquire, and process the images has been previously described in detail (Bright et al., 1987). The system included a Universal microscope stand (Carl Zeiss, Inc., Thornwood, NY), a scanning stage (Carl Zeiss, Inc.), an intensified silicon intensified target camera (model No. 66; Dage-MTI, Inc., Michigan City, IN), and an image processor (VICOM Systems, Inc., San Jose, CA).

The excitation light was generated from a 12-V tungsten–halogen filament lamp, operated at a constant current of 7.8 A. The intensifier was operated at 6,500 V and the gain was adjusted to 20% of the maximum setting. A 63× water immersion Plan–Neofluor objective (1.2 NA; Carl Zeiss, Inc.) was used in all experiments. The microscope contained an epiilluminator, model No. IIIRS (Zeiss) which housed four filters sets. A second filter holder for the epiilluminator was used to provide the fifth filter set needed for five-parameter imaging.

The sealed Sykes–Moore cell chamber was placed in a customized heating stage (Rainin Instrument Co., Inc., Woburn, MA) which surrounded the chamber and provided the primary temperature control. A thermistor, threaded through a needle port in the chamber, controlled the internal chamber temperature to 37°C (± 0.2°C) via a custom microprocessor feedback controlled air curtain (Bright et al., 1987).

*Image Processing.* Sets of images (image and background) were acquired sequentially for each of the fluorophores. All images were recorded with the image processor, averaging 128 frames. Background-subtracted images were enhanced using a variety of image enhancement techniques including histogram stretching, unsharp masking, thresholding, and spatial filtering (Castleman, 1979).

The image of each cell parameter was displayed as a separate color in the composite images. To display vesicles in a yellow color, the vesicle image was added to both the actin image (green channel) and the mitochondria image (red channel). The nuclei were placed in the blue channel. Simultaneous display of the red, green, and blue inputs created a color image of four cellular parameters displayed in four colors.

## Results

### Multiple Spectral–Parameter Imaging

The development of multiple spectral–parameter imaging as a tool to quantify and to correlate multiple molecular parameters in living cells requires the integration of fluorescent probe chemistry (Waggoner, 1986); the microscope as a spectroscopic instrument (Bright et al., 1987); photodetector characteristics (Bright and Taylor, 1986); image processing and analysis (Castleman, 1979); and cell biology (Taylor et al., 1986). The first step was to make use of a wider region of the light spectrum to optimize the ability to spectrally isolate one fluorescent probe at a time out of a total of at least five probes. Therefore, we chose four commercially available fluorescent probes that exhibited excitation and emission spectra ranging from the ultraviolet to the red and developed one new fluorescent probe that extended the usable spectrum from the far red into the near infrared (Fig. 1) (Ernst, L. A., R. K. Gupta, R. B. Mujumdar, and A. S. Waggoner; Mujumdar, R. B., L. A. Ernst, S. R. Mujumdar, and A. S. Waggoner, manuscripts submitted for publication). Filter sets were then designed to optimize the isolation of each fluorescent probe (Table I). Carefully selected band-pass filters reduced the small overlap in excitation regions and ensured distinct wavelength emissions for each probe.

---

*Figure 2.* Five-parameter imaging of spectrally distinct fluorescent probes within the same living Swiss 3T3 fibroblast. (*a*) Nuclei (blue): Hoechst 33342; (*b*) actin (green): AF-actin; (*c*) endosomes (yellow): lissamine rhodamine-B-dextran; (*d*) mitochondria (orange-red): diIC₁(5); (*e*) cell volume indicator (cyan): Cy7-dextran; (*f*) four-parameter composite of images *a–d* generated by digital image processing (see Materials and Methods). Bar, 8 µm.

1616
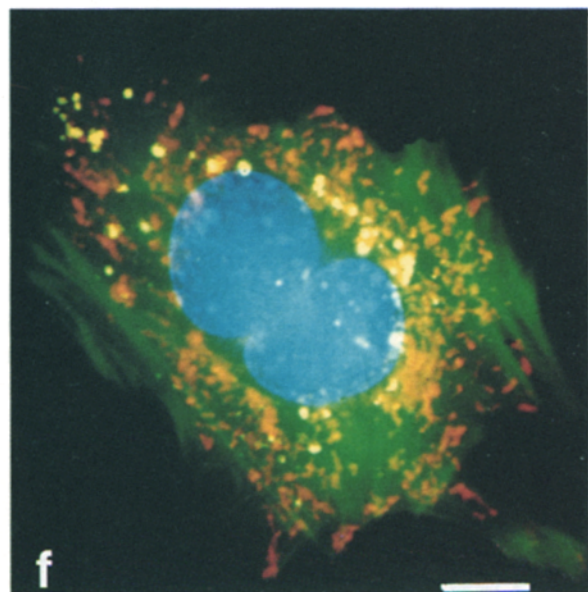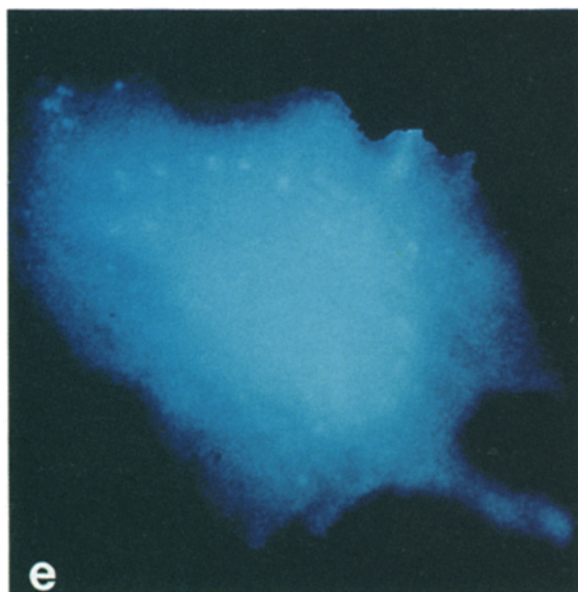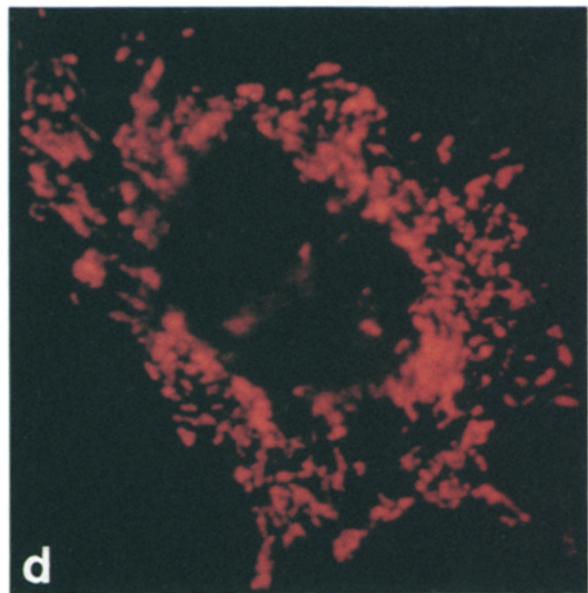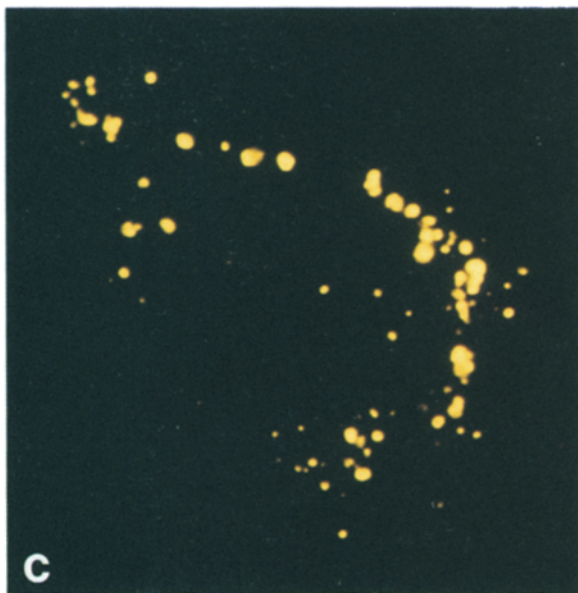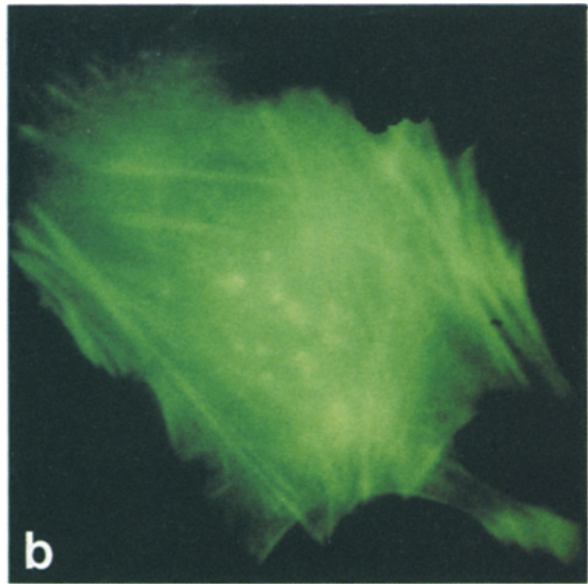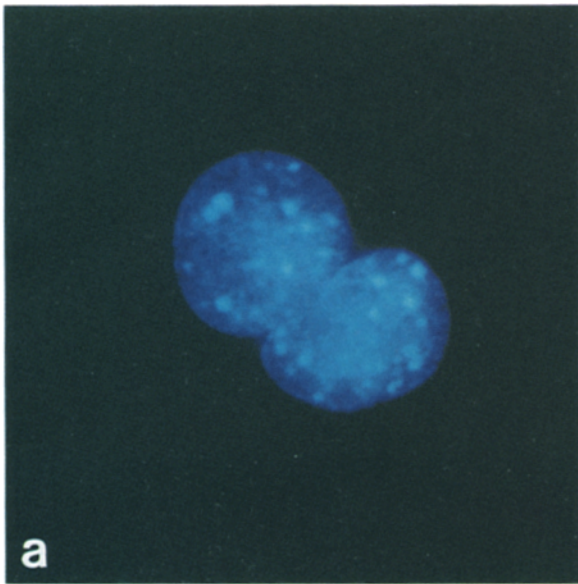
The digital imaging microscope system originally developed for ratio imaging of two excitation wavelengths (Tanasugarn et al., 1984; Bright et al., 1987) was modified for multiple excitation and emission capabilities. The present system required the manual movement of the filter holder of the epi-illuminator to step through the four filter sets, and an exchange of an additional inner filter holder was necessary to insert the fifth filter set. The small dynamic range of the intensified silicon intensified target camera at a fixed gain and high voltage setting required the adjustment of the excitation intensity with neutral density filters to keep each fluorescent probe image on scale. Furthermore, no attempt was made in this study to correct each image for spectrally dependent imaging characteristics (see Discussion for future technical improvements).

Five separate physiological parameters were chosen for this initial study based on both the ability to select a proper fluorescent probe that could be spectrally isolated from four other probes, and the potential importance of each physiological parameter in spatial and temporal changes during polarized cell movements. The following fluorescent probes and physiological parameters were selected: Hoechst 33342 for the nucleus (DNA); fluorescein-labeled actin as a fluorescent analog of actin; lissamine rhodamine-B-dextran for a marker of endosomes; diIC$_1$(5) for an indicator of mitochondria; and Cy7-dextran for a volume indicator. Fig. 2, a-e demonstrates that each parameter can be imaged separately.

The cell in Fig. 2 was a well-spread living binucleated Swiss 3T3 cell. The binuclei were localized in the center of the cell (Fig. 2 a); the actin exhibited areas of diffuse fluorescence as well as extensive stress fibers characteristic of well-spread, relatively nonmotile fibroblasts (Fig. 2 b); endosomes were distributed throughout the cell, but were concentrated in the perinuclear region (Fig. 2 c); mitochondria were dispersed throughout the cytoplasm (Fig. 2 d); and the volume indicator indicated that the volume and the pathlength varied across the cell diameter (Fig. 2 e). The nuclei were also labeled by the volume indicator due to the penetration of the small (10,000-mol-wt) labeled dextran through the nuclear pores (Luby-Phelps et al., 1986; Paine and Horowitz, 1980). The low light levels of excitation did not cause any adverse effects on the cells. The nuclei, actin, endosomes, and mitochondria were displayed together in order to correlate the distribution of each organelle (Fig. 2 f). The fifth parameter, the volume indicator, was not added to the composite image because the diffuse fluorescence pattern detracted from the clarity of the displayed organelle distribution. Computerized manipulation of the single images allowed the selection of groups of parameters for composite display to provide additional correlations (i.e., volume, actin, nucleus; volume, mitochondria, endosomes, nucleus; etc.). The choice of fluorescent probes (Table II) coupled with multiple spectral parameter imaging provides a method to obtain temporal and spatial information with quantitative measurements and correlations of several selected parameters.

## Wound Healing

We have used the in vitro wound-healing model to generate polarized movements of fibroblasts (Todaro, 1967; Gotleib et al., 1979). This model system is excellent for studying the many physiological parameters involved in the mechanisms of cell movement since motile fibroblasts are large and relatively slow moving.

Immediately after producing a wound, the cells exhibited the morphology of confluent cells; the nucleus was centrally located, actin was organized into stress fibers, and endosomes as well as mitochondria were distributed throughout the cell. Within 3 h, actively migrating cells along the edge of a wound exhibited a polarized structure with the nucleus in the rear of the cell (Fig. 3 a). The endosomes and mitochondria were repositioned around the front side of the nucleus facing the direction of migration. During this early stage of wound healing, both the labeled endosomes and the mitochondria were excluded from the lamellipodia (Fig. 3). Actin-based stress fibers remained in the rear of the migrating cell. The region directly behind the spreading lamellipodia contained fewer defined actin stress fibers, and the thin lamellipodia displayed primarily diffuse fluorescence indicating less organized actin (arrow in Fig. 3 a).

The cells exhibited a dramatic change between 3 and 7 h after producing the wound. Individual cells expressed the morphological changes at different times so that a continuum of the transformation could usually be seen along a wound. The cells became elongated, highly motile, and they continued to carry the nuclei in the rear of the cells. These locomoting cells did not have detectable actin stress fibers. However, in this later time period, both the labeled endosomes and the mitochondria moved out into the lamellipodia and could even approach the leading edges of the cells (Fig. 3 b). Mitochondria appeared to become concentrated in some extensions (arrow in Fig. 3 b).

## Discussion

### Multiple Spectral-Parameter Imaging

The value of quantitative fluorescence microscopy is due to its sensitivity, specificity, spatial, as well as temporal resolution, coupled with its capability to perform spectroscopic measurements. The sensitivity of fluorescence methods results from the large signal-to-noise ratio of fluorescence compared to methods such as absorption spectroscopy (Barak and Webb, 1981; Mathies and Stryer, 1986; Bright and Taylor, 1986). Specificity is expressed in two ways: (a) Individual molecules or organelles can be specifically labeled either by covalent reactions or by the use of high affinity, noncovalent probes (Taylor and Wang, 1980; Waggoner, 1986);

*Figure 3.* Four-parameter fluorescence imaging of Swiss 3T3 fibroblasts migrating into a "wound." (See Fig. 2, a-d for labeled parameters and color scheme). All cells displayed labeled mitochondria, endosomes, and nuclei, but only the cells along the wound edge were microinjected with actin. (a) Early cell migration (~3 h post-wounding) demonstrated the presence of actin, the loss of actin stress fibers, and the absence of endosomes and mitochondria in the extending lamella (arrow). (b) Late migration (~7 h post-wounding) demonstrated the continued presence of actin without stress fibers. The nuclei maintained a posterior position in the migrating cells, while the endosomes and mitochondria penetrated into the leading edge (arrow). Bar, 10 μm.
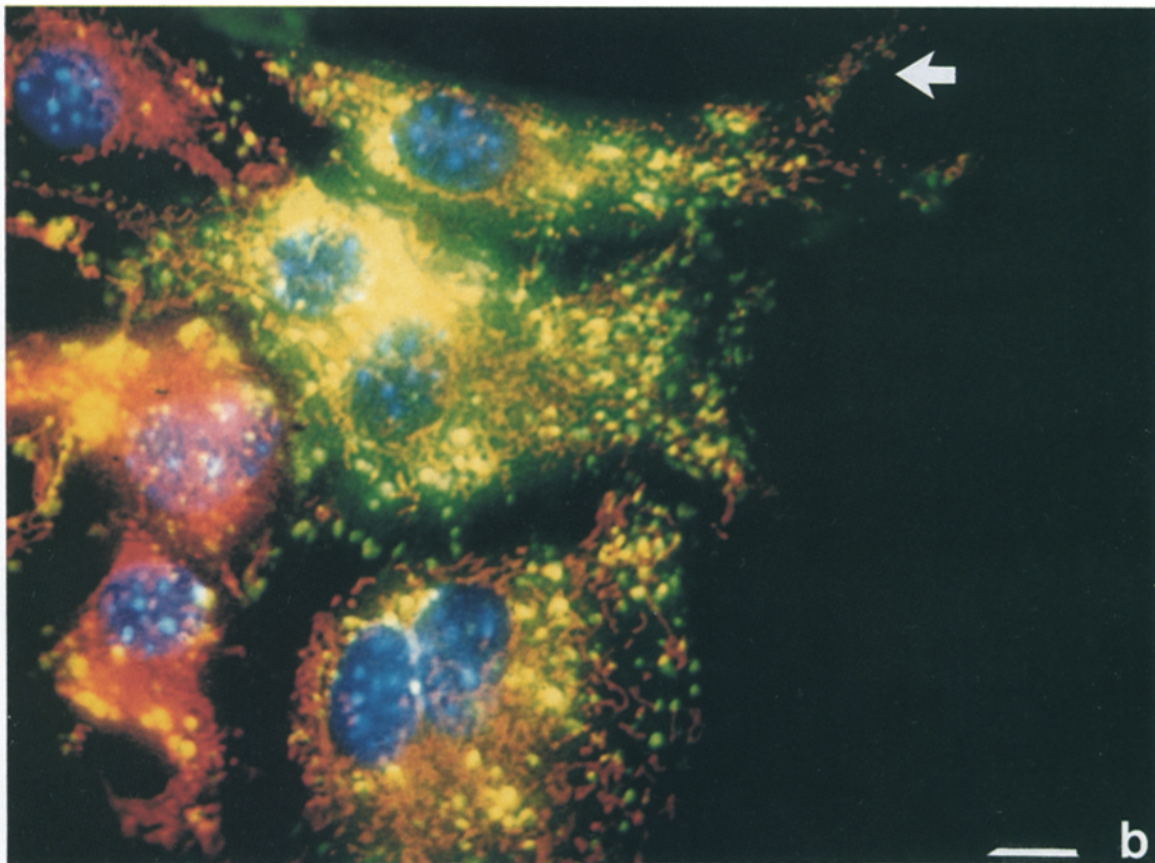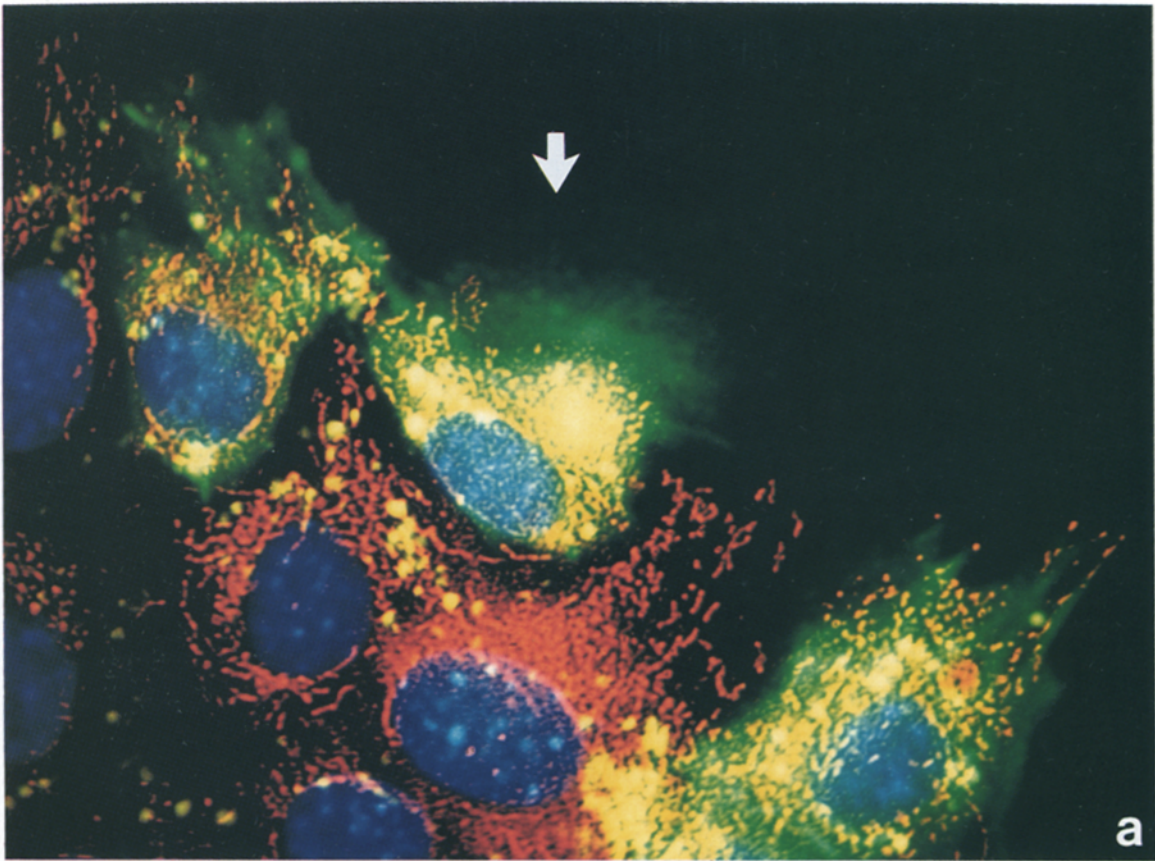
and (b) it is possible to analyze distinct fluorophores that are excited and emit fluorescence across the light spectrum, even in a mixture of fluorophores, by the proper selection of the fluorescent probes, filters, and detectors. The spatial resolution is limited by the physical optics of light microscopy, but the detectability of structures can extend well below these limits (see Allen et al., 1981; Inoue, 1981). The temporal resolution is determined by the lifetime of the excited state of the fluorescent molecules. The most commonly used probes allow the measurement of events occurring at the rate of $\sim 10^8$/s when a fast response photodetector like a photomultiplier is used.

The proper selection of fluorescent probes and optimal filters for the microscope permits the measurement of the dynamics of membrane potential (Waggoner, 1986; Gross et al., 1986), free calcium ion concentration (Poenie et al., 1986; Ratan et al., 1986; Fay et al., 1986), cytoplasmic and organeller pH (Heiple and Taylor, 1980; Tanasugarn et al., 1984; Bright et al., 1987; Tycko and Maxfield, 1982), DNA content (Latt et al., 1984), mitochondrial membrane potential (Johnson et al., 1981; Waggoner et al., 1985), fluorescent analogs of lipids (Pagano and Longmuir, 1983; Pagano and Sleight, 1985), proteins (Wang et al., 1982; Kreis and Birchmeier, 1983; Taylor et al., 1984, 1986), and a wide variety of other biologically active molecules (Table II). The use of fluorescence spectroscopic measurements such as resonance energy transfer, fluorescence anisotropy, total internal reflection fluorescence, and 3-D reconstruction can extend the use of multiple-parameter fluorescence microscopy (Lanni, 1986; Taylor et al., 1986).

The results of five-parameter fluorescence imaging emphasize the importance of integrating technology from the fields of fluorescence probe chemistry, the biology of fluorescence analogs, cell physiology, and digital imaging. Fig. 1 depicts the importance of selecting or preparing a battery of fluorescent probes that span a wide range of the ultraviolet, visible, and near-infrared spectrum. It is now possible to select up to five parameters by spectral isolation (Table I), while the development of more probes in the far red and infrared region of the spectrum could increase the total number of spectral parameters (Waggoner, 1986). The feasibility of multiple spectral analysis of five fluorescent probes in the same living 3T3 cell is demonstrated in Fig. 2, a–e.

The instrumentation for multiple-parameter fluorescence imaging microscopy evolved from the two-wavelength ratio imaging system (Tanasugarn et al., 1984), and modifications to this system included automated computer control over most of the microscope functions (Bright et al., 1987). The optimal use of multiple spectral parameter fluorescence imaging will require further developments in the microscope, microscope peripheral controls, photodetectors, and image processing. Automated corrections for spectral sensitivity, linearity, and shading of the photodetectors, as well as corrections for wavelength-dependent variations in magnification, focus, image registration, and geometric distortion, will increase the value of multiple spectral parameter fluorescence imaging microscopy. The use of fluorescence imaging microscopy optimizes the acquisition of spatial information, while it limits the acquisition of very fast transient events (Bright and Taylor, 1986; Bright et al., 1987). A quantitative fluorescence microscope system possessing both imaging and photometric capabilities can access both the highest spatial and temporal information from fluorescent probes.

Although the maximum power of fluorescence microscopy can be attained with live cells by investigating cellular processes in time and space (Taylor et al., 1986), multiple parameter analysis can also be applied to fixed cell preparations. This application is simply an extension of traditional immunofluorescence where multiple antibodies, nucleic acid hybridization probes, and other fluorescent cytochemical probes, suitably labeled, could be co-mapped in single cells. Furthermore, at low total magnification, cell populations could be analyzed using spectral isolation to determine the population statistics of reactivity to multiple probes.

## Cell Migration during Wound Healing

The migration of fibroblasts into an in vitro wound is a cellular process that probably involves multiple cell functions that must be integrated in time and space (Vasiliev, 1985; Trinkaus, 1985). The cell functions are not limited to, but probably include (a) signal processing at the cell surface involving receptors and ligands for chemical and/or mechanical stimulus–response coupling; (b) signal transduction across the membrane involving ionic changes and/or biochemical modification of molecules in the signal pathway; (c) cell polarity determinants such as the reorientation of the microtubule-organizing center and Golgi region coupled with localized membrane insertion (Abercrombie et al., 1970; Bergmann et al., 1983); (d) control of cell adhesion and de-adhesion from the cell substrate (Izzard et al., 1985); (e) generation of force within the cytoplasm (Chen, 1981; Trinkaus, 1985); and (f) the production of energy to power all of the active processes.

This study and previous investigations indicate that polarized movement during wound healing occurs in stages. Fibroblasts in a confluent monolayer do not have any obvious polarity of cell shape or distribution or organelles, and actin forms extensive stress fibers. Within 3 h after the production of a wound, the cells along the edge of the wound become polarized in both cell shape and the distribution of some organelles as well as exhibiting changes in the organization of cytoskeletal proteins (Heggeness et al., 1977; Gotleib et al., 1979). The transformation of actin from stress fibers into less organized structures (Figs. 2 b and 3 a and b) is characteristic of the initiation of cell movement (Taylor et al., 1980a; Herman et al., 1981). Kupfer et al. (1982) demonstrated that the microtubule-organizing center and Golgi region reorient to the side of the cell facing the wound in a majority of cells within 5 h after producing a wound. Bergmann et al. (1983) also showed evidence that membrane was inserted at the leading edge of cells at the edge of a wound. These observations have been used to support the concept that part of the extension of lamellipodia could arise from polarized membrane insertion (Abercrombie et al., 1970; Bergman et al., 1983). However, neither labeled endosomes nor mitochondria penetrate into the extending lamellipodia during the first phase of cell polarization which lasts several hours (arrow in Fig. 3 a). In addition labeled ficolls with a calculated diameter of 50 nm are also relatively excluded from the forming lamellipodia during this phase (Luby-Phelps, K., and D. L. Taylor, manuscript in preparation). Therefore, any

membrane traffic probably occurs as actively transported small vesicles. It is possible that the reorientation of the microtubule-organizing center and Golgi region, preceding the formation of the extending lamellipodia, is required to orient microtubules toward the leading edge of cells at the wound (Heggeness et al., 1977). A microtubule-based transport of Golgi-derived vesicles could then direct the hypothesized vesicles to the leading edge. This mechanism would be analogous to the anterograde transport of vesicles in axons (Allen et al., 1982). This model can be tested directly using a combination of multiple-spectral parameter imaging and video-enhanced contrast microscopy.

Any mechanism for the early extension of lamellipodia must account for the presence of a dense meshwork of actin filaments (Small, 1981; Bridgeman et al., 1986), the absence of large organelles, and the low diffusion of particles larger than ∼50-nm diameter (Luby-Phelps, K., and D. L. Taylor, manuscript in preparation). The protrusion of lamellipodia could be caused by one or more mechanisms including (a) actin assembly (Tilney and Kallenback, 1979; Wang, 1985); (b) turgor pressure in the lamellipodia caused by solation of a gel (Oster, 1984; Taylor et al., 1980a, b); (c) turgor pressure generated by the contraction of the tail (Chen, 1981; Taylor et al., 1980a, b); and/or (d) local contractions.

The later phase of polarized movements during wound healing occurs at variable times after producing the wound. However, most cells are actively translocating after 7 h (Fig. 3 b). During this stage, locomoting cells displayed less organized actin throughout the elongated cells. In addition to the active translocation of cells, the labeled endosomes and mitochondria penetrate into the extending lamellipodia (Fig. 3 b). Therefore, a major change in the structure and/or chemistry of the lamellipodial cytoplasm occurs between the early phase of wound healing and this later phase. This transition must be investigated in terms of possible changes in ionic conditions, organization of the cytoskeleton and contractile proteins, and the physiological activity of specific organelles.

Multiple-spectral parameter imaging (see Table II) should facilitate the understanding of complex cellular processes like cell migration during wound healing. Future developments of new fluorescent, delayed fluorescent, and phosphorescent probes, along with advances in instrumentation, will extend the power of this approach.

References

Abercrombie, M., J. E. M. Heaysman, and S. M. Pegrum. 1970. The locomotion of fibroblasts in culture. III. Movements of particles on the dorsal surface of the leading lamella. Exp. Cell Res. 62:389–398.

Agard, D. A., and J. W. Sedat. 1983. Three-dimensional architecture of a polytene nucleus. Nature (Lond.). 302:676–681.

Allen, R. D., and N. S. Allen. 1983. Video-enhanced microscopy with a computer frame memory. J. Microsc. 129:3–17.

Allen, R. D., N. Stromgren Allen, and J. L. Travis. 1981. Video-enhanced contrast, differential interference contrast (AVEC-DIC) microscopy: a new method capable of analyzing microtubule-related motility in the reticulopodial network of Allogromia laticollaris. Cell Motil. 1:291–302.

Allen, R. D., J. Metuzals, I. Tasaki, S. T. Brady, and S. P. Gilbert. 1982. Fast axonal transport in squid giant axon. Science (Wash. DC). 218:1127–1129.

Amato, P. A., E. R. Unanue, and D. L. Taylor. 1983. Distribution of actin in spreading macrophages: a comparative study on living and fixed cells. J. Cell Biol. 96:750–761.

Arndt-Jovin, D. J., M. Robert-Nicoud, S. J. Kaufman, and T. M. Jovin. 1985. Fluorescence digital imaging microscopy (DIM) in cell biology. Science (Wash. DC). 230:247–256.

Axelrod, D., D. E. Koppel, J. Schlessinger, E. Elson, and W. W. Webb. 1976. Mobility measurement by analysis of fluorescence photobleaching recovery kinetics. Biophys. J. 16:1005–1069.

Barak, L. S., and W. W. Webb. 1981. Fluorescent low density lipoprotein for observation of dynamics of individual receptor complexes on cultured human fibroblasts. J. Cell Biol. 90:595–604.

Benson, D. M., J. Bryan, A. L. Plant, A. M. Gotto, Jr., and L. C. Smith. 1985. Digital imaging fluorescence microscopy: spatial heterogeneity of photobleaching rate constants in individual cells. J. Cell Biol. 100:1309–1323.

Bergmann, J. E., A. Kupfer, and S. J. Singer. 1983. Membrane insertion at the leading edge of motile fibroblasts. Proc. Natl. Acad. Sci. USA. 80:1367–1371.

Bridgeman, P. C., B. Kachar, and T. S. Reese. 1986. The structure of cytoplasm in directly frozen cultured cells. II. Cytoplasmic domains associated with organelle movements. J. Cell Biol. 102:1510–1521.

Bright, G. R., and D. L. Taylor. 1986. Imaging at low light level in fluorescence microscopy. In Applications of Fluorescence in the Biomedical Sciences. D. L. Taylor, A. S. Waggoner, R. F. Murphy, F. Lanni, and R. R. Birge, editors. Alan R. Liss, Inc., New York. 257–288.

Bright, G. R., G. W. Fisher, J. Rogowska, and D. L. Taylor. 1987. Fluorescence ratio imaging microscopy: temporal and spatial measurements of cytoplasmic pH. J. Cell Biol. 104:1019–1033.

Castleman, K. R. 1979. Digital Image Processing. Prentice-Hall Inc., Englewood Cliffs, NJ.

Chance, B. 1963. Localization of intracellular and intramitochondrial compartments. Ann. N.Y. Acad. Sci. 108:322–330.

Chen, W.-T. 1981. Mechanism of the retraction of the trailing edge during fibroblast movement. J. Cell Biol. 90:187–200.

Cohen, R. L., K. A. Muirhead, J. E. Gill, A. S. Waggoner, and P. K. Horan. 1981. A cyanine dye distinguishes between cycling and non-cycling fibroblasts. Nature (Lond.). 290:593–595.

Fay, F., K. Fogarty, and J. Coggins. 1986. The analysis of molecular distribution in single cells using a digital imaging microscope. In Optical Methods in Cell Physiology. P. deWeer and B. Salzburg, editors. John Wiley & Sons, Inc., New York. 51–63.

Gotlieb, A., M. H. Heggeness, J. F. Ash, and S. J. Singer. 1979. Mechanochemical proteins, cell motility, and cell-cell contacts: the localization of mechanochemical proteins inside cultured cells at the leading edge of an in vitro "wound". J. Cell. Physiol. 100:563–578.

Gross, D., L. M. Loew, and W. W. Webb. 1986. Optical imaging of cell membrane potential changes induced by applied electric fields. Biophys. J. 50:339–348.

Heggeness, M. H., K. Wang, and S. J. Singer. 1977. Intracellular distributions of mechanochemical proteins in cultured fibroblasts. Proc. Natl. Acad. Sci. USA. 74:3883–3887.

Heiple, J. M., and D. L. Taylor. 1980. Intracellular pH in single motile cells. J. Cell Biol. 86:885–890.

Herman, I. M., N. J. Crisona, and T. D. Pollard. 1981. Relation between cell activity and the distribution of cytoplasmic actin and myosin. J. Cell Biol. 90:84–91.

Inoue, S. 1981. Video image processing greatly enhances contrast, quality, and speed in polarization-based microscopy. J. Cell Biol. 89:346–356.

Izzard, C. S., S. L. Izzard, and J. A. DePasquale. 1985. Molecular basis of cell-substrate adhesions. Exp. Biol. Med. 10:1–22.

Jacobson, K., E. Wu, and G. Poste. 1976. Measurement of the translational mobility of concanavalin A in glycerol-saline solutions, and on the cell surface by fluorescence recovery after photobleaching. Biochim. Biophys. Acta. 433:215–222.

Johnson, L. V., M. L. Walsh, B. J. Bockus, and L. B. Chen. 1981. Monitoring of relative mitochondrial membrane potential in living cells by fluorescence microscopy. J. Cell Biol. 88:526–535.

Kohen, E., B. Thorell, J. Hirshberg, A. Woiters, C. Kohen, P. Bartick, J. M. Salmon, P. Viallet, D. Schahtschabel, A. Rabinovitch, D. Minty, P. Meda, H. Westerhoff, J. Nestor, and J. Ploem. 1981. Microspectrofluorometric procedures and their applications in biological systems. In Modern Fluorescence Spectroscopy. E. L. Wehry, editor. Plenum Press, New York. 295–346.

Kreis, T., and W. Birchmeier. 1983. Microinjection of fluorescently labeled proteins into living cells with emphasis on cytoskeletal proteins. Int. Rev. Cytol. 75:209–228.

Kupfer, A., D. Lauvard, and S. J. Singer. 1982. Polarization of the golgi apparatus and the microtubule-organizing center in cultured fibroblasts at the edge of an experimental wound. Proc. Natl. Acad. Sci. USA. 79:2603–2607.

Lanni, F. 1986. New aspects of microscopy in cell biology. In Applications of Fluorescence in the Biomedical Sciences. D. L. Taylor, A. S. Waggoner, R. F. Murphy, F. Lanni, and R. R. Birge, editors. Alan R. Liss, Inc., New York. 449–459.

Latt, S. A., M. Marino, and M. Lalande. 1984. New fluorochromes, compatible with high wavelength excitation for flow cytometric analysis of cellular nucleic acids. *Cytometry.* 5:339–347.

Luby-Phelps, K., D. L. Taylor, and F. Lanni. 1986. Probing the structure of cytoplasm. *J. Cell Biol.* 102:2015–2022.

Mathies, R. A., and L. Stryer. 1986. Single-molecule fluorescence detection: a feasibility study using phycoerythrin. *In* Applications of Fluorescence in the Biomedical Sciences. D. L. Taylor, A. S. Waggoner, R. F. Murphy, F. Lanni, and R. R. Birge, editors. Alan R. Liss, Inc., New York. 129–140.

McNeil, P. L., R. F. Murphy, F. Lanni, and D. L. Taylor. 1984. A method for incorporating macromolecules into adherent cells. *J. Cell Biol.* 98:1556–1564.

Oster, G. F. 1984. On the crawling of cells. *J. Embryol. Exp. Morphol.* 83:329–364.

Pagano, R. E., and K. J. Longmuir. 1983. Intracellular translocation and metabolism of fluorescent lipid analogs in cultured mammalian cells. *Trends Biochem. Sci.* 8:157–161.

Pagano, R. E., and R. G. Sleight. 1985. Defining lipid transport pathways in animal cells. *Science (Wash. DC).* 229:1051–1057.

Paine, P. L., and S. B. Horowitz. 1980. The movement of material between nucleus and cytoplasm. *In* Cell Biology: A Comprehensive Treatise. Vol. 4. L. Goldstein, and D. M. Prescott, editors. Academic Press, Inc., New York. 299–338.

Poenie, M., J. Alderton, S. Steinhardt, and R. Tsien. 1986. Calcium rises abruptly and briefly throughout the cell at the onset of anaphase. *Science (Wash. DC.).* 233:886–889.

Ratan, R. R., M. L. Shelanski, and F. R. Maxfield. 1986. Transition from metaphase to anaphase is accompanied by local changes in cytoplasmic free calcium in PtK2 kidney epithelium cells. *Proc. Natl. Acad. Sci. USA.* 85:5136–5140.

Reynolds, G. T., and D. L. Taylor. 1980. Image intensification applied to light microscopy. *Bioscience.* 9:586–592.

Rose, B., and W. Loewenstein. 1975. Calcium ion distribution in cytoplasm visualized by aequorin: diffusion in cytosol restricted by energized sequestering. *Science (Wash. DC.).* 190:1204–1206.

Salmon, E. D., and P. Wadsworth. 1986. Fluorescence studies of tubulin and microtubule dynamics in living cells. *In* Applications of Fluorescence in the Biomedical Sciences. D. L. Taylor, A. S. Waggoner, R. F. Murphy, F. Lanni, and R. R. Birge, editors. Alan R. Liss, Inc., NY. 377–403.

Small, J. V. 1981. Organization of actin in the leading edge of cultured cells: influence of osmium tetroxide and dehydration on the ultrastructure of actin meshwork. *J. Cell Biol.* 91:695–705.

Tanasugarn, L., P. McNeil, G. T. Reynolds, and D. L. Taylor. 1984. Microspectrofluorometry by digital image processing: measurement of cytoplasmic pH. *J. Cell Biol.* 98:717–724.

Taylor, D. L., and Y.-L. Wang. 1978. Molecular cytochemistry incorporation of fluorescently labeled actin into living cells. *Proc. Natl. Acad. Sci. USA.* 75:857–861.

Taylor, D. L., and Y.-L. Wang. 1980. Fluorescently labeled molecules as probes of the structure of living cells. *Nature (Lond.).* 284:405–410.

Taylor, D. L., P. A. Amato, K. Luby-Phelps, and P. McNeil. 1984. Fluorescent analog chemistry. *Trends Biochem. Sci.* 9:88–91.

Taylor, D. L., P. A. Amato, P. L. McNeil, K. Luby-Phelps, and L. Tansaugarn. 1986. Spatial and temporal dynamics of specific molecules and ions in living cells. *In* Applications of Fluorescence in the Biomedical Sciences. D. L. Taylor, A. S. Waggoner, R. F. Murphy, F. Lanni, and R. R. Birge, editors. Alan R. Liss, Inc., NY. 347–376.

Taylor, D. L., J. Blinks, and G. T. Reynolds. 1980a. Contractile basis of ameboid movement. VIII. Aequorin luminescence during ameboid movement, endocytosis, and capping. *J. Cell Biol.* 86:599–607.

Taylor, D. L., Y. L. Taylor, and J. Heiple. 1980b. Contractile basis of ameboid movement. VII. Distribution of fluorescently labeled actin in living amoebae. *J. Cell Biol.* 86:590–598.

Tilney, L. G., and N. Kallenbach. 1979. Polymerization of actin. VI. The polarity of the actin filaments in the acrosomal process and how it might be determined. *J. Cell Biol.* 81:608–623.

Todaro, G., Y. Matsuya, S. Bloom, A. Robbins, and H. Green. 1967. *In* Growth Regulating Substances for Animal Cells in Culture. V. Defendi, and M. Stoker, editors. Wistar Institute Press, Philadelphia, PA. Wistar Institute Symposium. 7:87–98.

Trinkaus, J. P. 1985. Protrusive activity of the cell surface and the initiation of cell movement during morphogenesis. *Exp. Biol. Med.* 10:130–173.

Tsien, R., T. Pozzan, and T. Rink. 1982. Calcium homeostasis in intact lymphocytes: cytoplasmic free calcium monitored with new, intracellularly trapped fluorescent indicator. *J. Cell Biol.* 94:325–334.

Tycko, B., and F. R. Maxfield. 1982. Rapid acidification of endocytotic vesicles containing alpha-2-macroglobulin. *Cell.* 28:643–651.

Vasiliev, J. M. 1985. Spreading of non-transformed and transformed cells. *Biochim. Biophys. Acta.* 780:21–65.

Waggoner, A. S. 1979. Dye indicators of membrane potential. *Annu. Rev. Biophys. Bioeng.* 8:47.

Waggoner, A. S. 1985. Dye probes of cell organelle and vesicle membrane potentials. *In* The Enzymes of Biological Membranes. A. Martonosi, editor. Plenum Press, NY. 313–331.

Waggoner, A. S. 1986. Fluorescent probes for analysis of cell structure, function and health by flow and imaging cytometry. *In* Applications of Fluorescence in the Biomedical Sciences. D. L. Taylor, A. S. Waggoner, R. F. Murphy, F. Lanni, and R. R. Birge, editors. Alan R. Liss, Inc., New York. 3–28.

Wang, Y.-L. 1985. Exchange of actin subunits at the leading edge of living fibroblasts: a possible role of treadmilling. *J. Cell Biol.* 101:597–602.

Wang, Y.-L., and D. L. Taylor. 1980. Preparation and characterization of a new molecular cytochemical probe: 5-iodoacetamidofluorescein labeled actin. *J. Histochem.* 28:1198–1206.

Wang, Y.-L., J. Heiple, and D. L. Taylor. 1982. Fluorescent analog chemistry of contractile proteins. *Methods Cell Biol.* 25:(Pt. B):1–11.

West, S. S. 1969. Fluorescence microspectrophotometry of supravitally stained cells. *In* Physical Techniques in Biological Research. Vol. 3. A. W. Pollister, editor. 253–321.

Willingham, M., and I. Pastan. 1978. The visualization of fluorescent proteins in living cells by video intensification microscopy. *Cell.* 13:501–505.